Chapter 1

Surface Friction and Boundary Layer Thickening in Transitional Flow

Ping Lu, Manoj Thapa and Chaoqun Liu

Additional information is available at the end of the chapter

http://dx.doi.org/10.5772/53581

1. Introduction

Correct understanding of turbulence model, particularly boundary-layer turbulence model, has been a subject of significant investigation for over a century, but still is a great challenge for scientists[1]. Therefore, successful efforts to control the shear stress for turbulent boundary-layer flow would be much beneficial for significant savings in power requirements for the vehicle and aircraft, etc. Therefore, for many years scientists connected with the industry have been studying for finding some ways of controlling and reducing the skin-friction[2]. Experimentally, it has been shown that the surface friction coefficient for the turbulent boundary layer may be two to five times greater than that for laminar boundary layer[6]. By careful analysis of our new DNS results, we found that the skin-friction is immediately enlarged to three times greater during the transition from laminar to turbulent flow. We try to give the mechanism of this phenomenon by studying the flow transition over a flat plate, which may provide us an idea how to design a device and reduce shear stress.

Meanwhile, some of the current researches are focused on how to design a device that can artificially increase the thickness of the boundary layer in the wind tunnel. For instances, one way to increase is by using an array of varying diameter cross flow jets with the jet diameter reducing with distance downstream, and there are other methods like boundary layer fence, array of cylinders, or distributed drag method, etc. For detail information read [9]. However, there are few literatures which give the mechanism how the multi-level rings overlap and how boundary layer becomes thicker. By looking at the Figure 1 which is copied from the book of Schilichting, we can note that the boundary layer becomes thicker and thicker during the transition from laminar to turbulent flow. This phenomenon is also numerically proved by our DNS results by flow transition over a flat plate, which is shown in Figure 2 representing multiple level ring overlap. Moreover, we find that they never mix each other. More details will be given in the following sections.

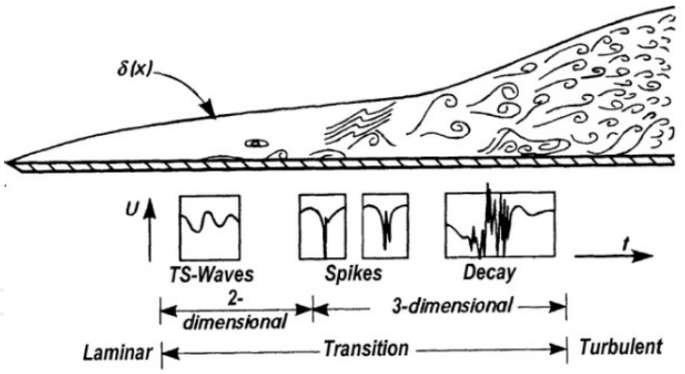

[16] (Copy of Figure 15.38, Page 474, Book of layer thickening Boundary Layer Theory by Schilichting et al, 2000)

Figure 1. Schematic of flow transition on a flat plate

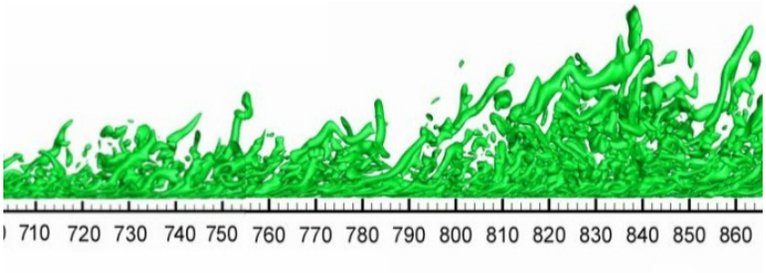

Figure 2. Vortex cycles overlapping and boundary

2. Case setup

The computational domain on a flat plate is displayed in Figure 3. The grid level is 1920x128x241, representing the number of grids in streamwise (x), spanwise (y), and wall normal (z) directions. The grid is stretched in the normal direction and uniform in the streamwise and spanwise directions. The length of the first grid interval in the normal direction at the entrance is found to be 0.43 in wall units $(z^+ = 0.43)$.

The parallel computation is accomplished through the Message Passing Interface (MPI) together with domain decomposition in the streamwise direction. The computational domain is partitioned into N equally-sized sub-domains along the streamwise direction. N is the number of processors used in the parallel computation. The flow parameters, including Mach number, Reynolds number, etc are listed in Table 1. Here, $x_{in} = 300.79\delta_{in}$ represents the distance between leading edge and inlet, $Lx = 798.03\delta_{in}$, $Ly = 22\delta_{in}$, $Lz_{in} = 40\delta_{in}$ are the lengths of the computational domain in x-, y-, and z-directions respectively and $T_w = 273.15K$ is the wall temperature.

M_∞	Re	x_{in}	Lx	Ly	Lz	T_w	T_∞
0.5	1000	300.79 δ_s	798.03 δ_{in}	22 δ_{in}	40 δ_{in}	273.15K	273.15K

Table 1. Flow parameters

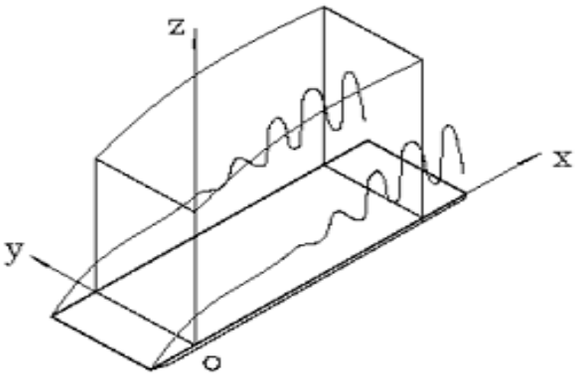

Figure 3. Computation domain

3. Code validation and DNS results visualization

To justify the DNS codes and DNS results, a number of verifications and validations have been conducted[5,12,13,14,15]

1. Comparison with Linear Theory

Figure 4(a) compares the velocity profile of the T-S wave given by our DNS results to linear theory. Figure 4(b) is a comparison of the perturbation amplification rate between DNS and LST. The agreement between linear theory and our numerical results is good.

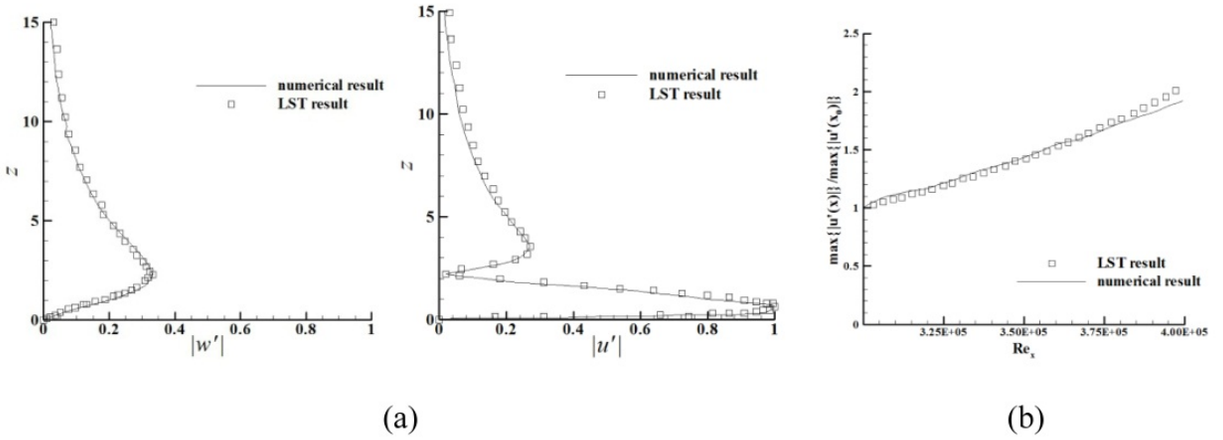

Figure 4. Comparison of the numerical and LST (a) velocity profiles at Rex=394300 (b) perturbation amplification rate

2. Skin friction and grid convergence

The skin friction coefficients calculated from the time-averaged and spanwise-averaged profiles on coarse and fine grids are displayed in Figure 5(a). The spatial evolution of skin friction coefficients of laminar flow is also plotted out for comparison. It is observed from these figures that the sharp growth of the skin-friction coefficient occurs after $x \approx 450\delta_{in}$, which is defined as the 'onset point'. The skin friction coefficient after transition is in good agreement with the flat-plate theory of turbulent boundary layer by Cousteix in 1989

(Ducros, 1996). The agreement between coarse and fine grid results also shows the grid convergence.

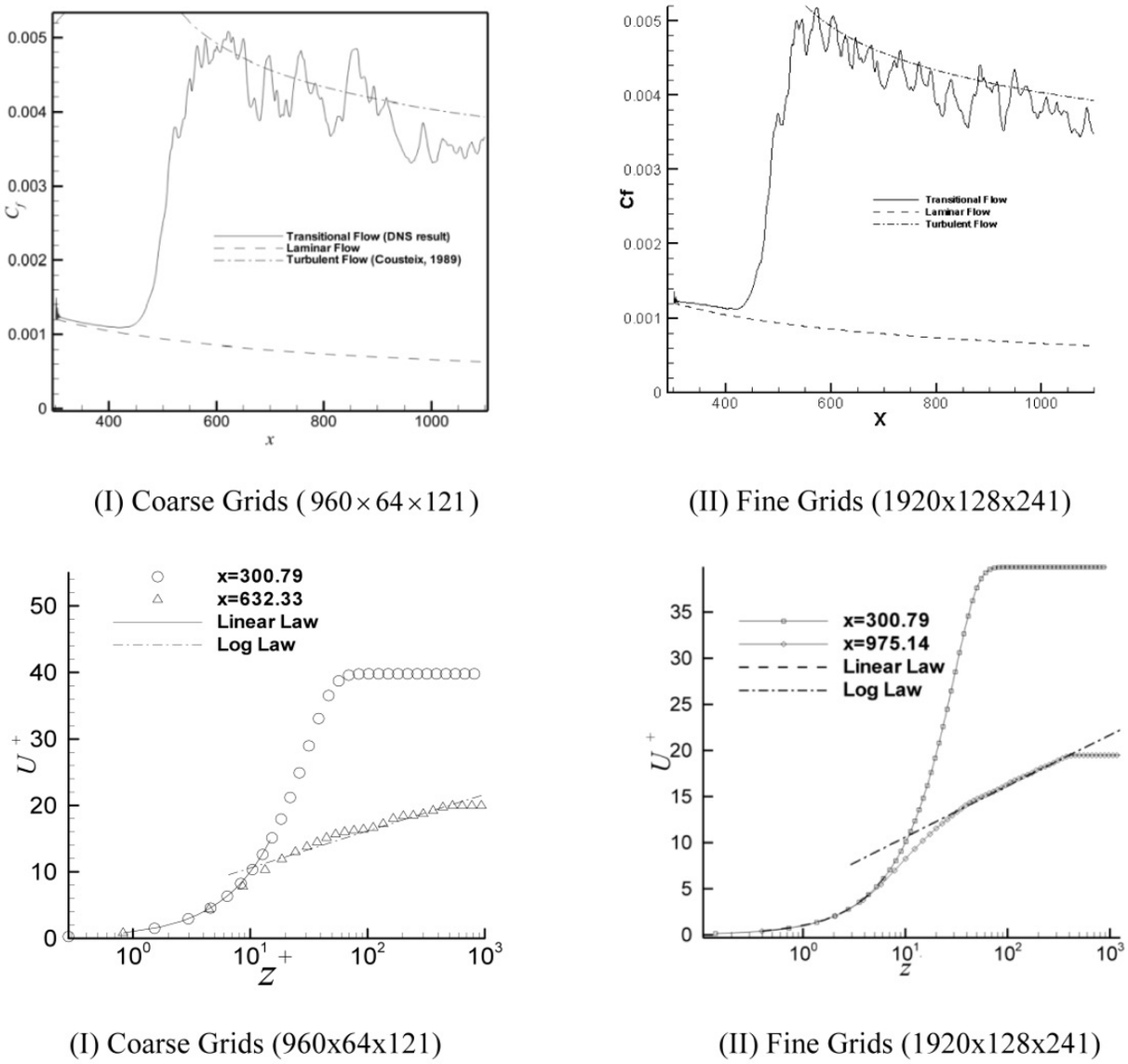

(I) Coarse Grids ($960 \times 64 \times 121$) (II) Fine Grids (1920x128x241)

(I) Coarse Grids (960x64x121) (II) Fine Grids (1920x128x241)

Figure 5. (a). Streamwise evolutions of the time-and spanwise-averaged skin-friction coefficient, (b). Log-linear plots of the time-and spanwise-averaged velocity profile in wall unit

3. Comparison with log law

Time-averaged and spanwise-averaged streamwise velocity profiles for various streamwise locations in two different grid levels are shown in Figure 5(b). The inflow velocity profiles at $x = 300.79\delta_{in}$ is a typical laminar flow velocity profile. At $x = 632.33\delta_{in}$, the mean velocity profile approaches a turbulent flow velocity profile (Log law). This comparison shows that the velocity profile from the DNS results is a turbulent flow velocity profile and the grid convergence has been realized. Figures 5(a) and 5(b) also show that grid convergence is obtained in the velocity profile.

4. Spectra and Reynolds stress (velocity) statistics

Figure 6 shows the spectra in x- and y- directions. The spectra are normalized by z at location of $\mathrm{Re}_x = 1.07 \times 10^6$ and $y^+ = 100.250$. In general, the turbulent region is approximately defined by $y^+ > 100$ and $y/\delta < 0.15$. In our case, The location of $y/\delta = 0.15$ for $\mathrm{Re}_x = 1.07 \times 10^6$ is corresponding to $y^+ \approx 350$, so the points at $y^+ = 100$ and 250 should be in the turbulent region. A straight line with slope of -5/3 is also shown for comparison. The spectra tend to tangent to the $k^{-\frac{5}{3}}$ law. The large oscillations of the spectra can be attributed to the inadequate samples in time when the average is computed.

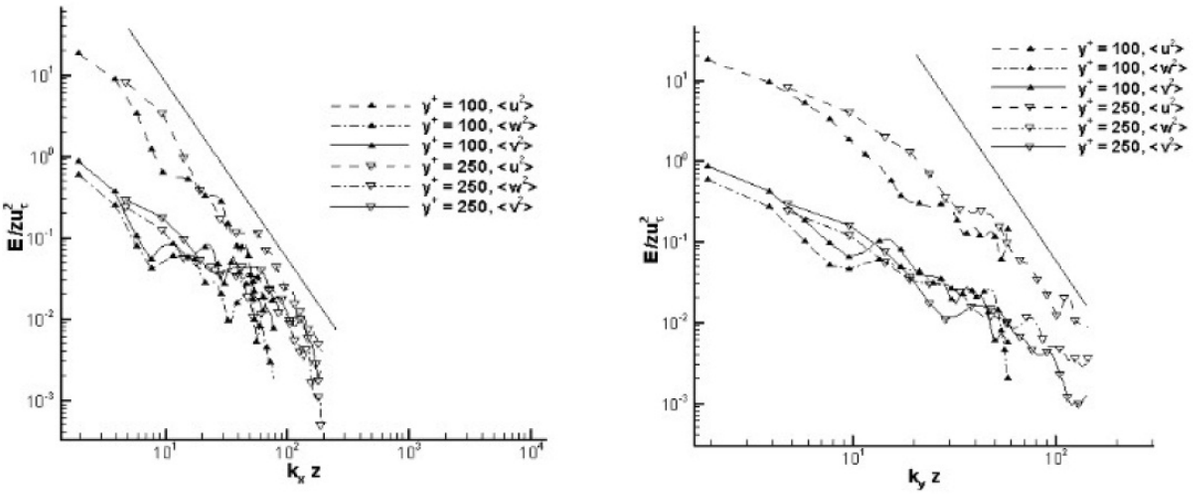

Figure 6. (a) Spectra in x direction; (b)Spectra in y direction

Figure 7 shows Reynolds shear stress profiles at various streamwise locations, normalized by square of wall shear velocity. There are 10 streamwise locations starting from leading edge to trailing edge are selected. As expected, close to the inlet where $\mathrm{Re}_x = 326.79 \times 10^3$ where the flow is laminar, the values of the Reynolds stress is much smaller than those in the turbulent region. The peak value increases with the increase of x. At around $\mathrm{Re}_x = 432.9 \times 10^3$, a big jump is observed, which indicates the flow is in transition. After $\mathrm{Re}_x = 485.9 \times 10^3$, the Reynolds stress profile becomes close to each other in the turbulent region. So for this case, we can consider that the flow becomes turbulent after $\mathrm{Re}_x = 490 \times 10^3$.

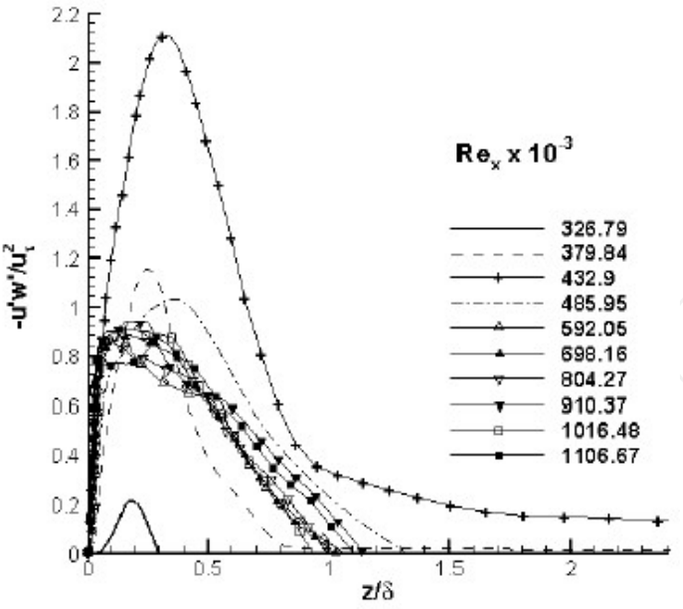

Figure 7. Reynolds stress

All these verifications and validations above show that our code is correct and our DNS results are reliable.

4. Small vortices generation and shape of positive spikes

A general scenario of formation and development of small vortices structures at the late stages of flow transition can be seen clearly by Figure 8.

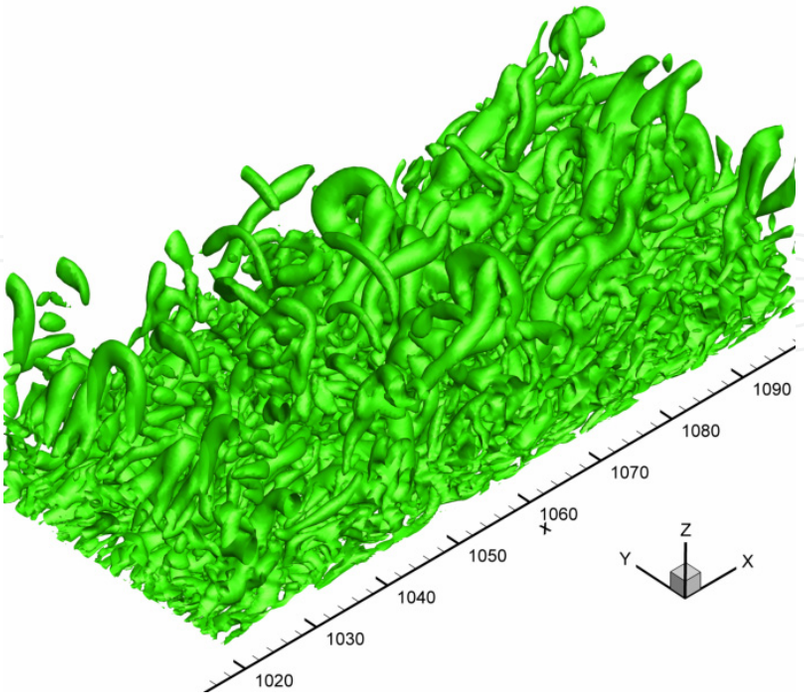

Figure 8. Visualization of flow transition at t=8.0T based on eigenvalue λ_2

Figure 9(a) is the visualization of λ_2 from the bottom view. Meanwhile, the shape of positive spikes along x-direction is shown in figure 9(b). We can see that from the top to bottom, originally the positive spike is generated by sweep motion, and then two spikes combine together to form a much stronger high speed area. Finally, two red regions (high speed areas) depart further under the ring-like vortex[5].

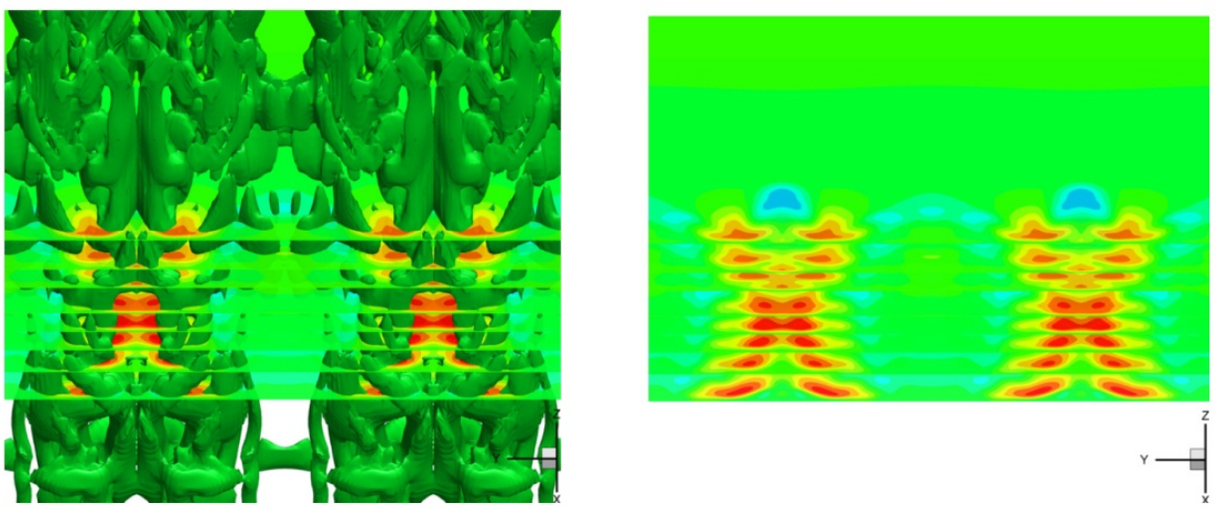

(a) (b)

Figure 9. (a) bottom view of λ_2 structure; (b) visulation of shape of positive spikes along x-direction

In order to fully understand the relation between small length scale generation and increase of the skin friction, we will focus on one of two slices in more details first.

The streamwise location of the negative and positive spikes and their wall-normal positions with the co-existing small structures can be observed in this section. Figures 10(a) demonstrates that the small length scales (turbulence) are generated near the wall surface in the normal direction, and Figure 10(b) is the contour of velocity perturbation at an enlarged section x=508.633 in the streamwise direction. Red spot at the Figure 10(b) indicates the region of high shear layer generated around the spike. It shows that small vortices are all generated around the high speed region (positive spikes) due to instability of high shear layer, especially the one between the positive spikes and solid wall surface. For more references see[7,14,15].

5. Control of skin friction coefficient

The skin friction coefficient calculated from the time-averaged and spanwise-averaged profile is displayed in Figure 11. The spatial evolution of skin friction coefficients of laminar flow is also plotted out for comparison. It is observed from this figure that the sharp growth of the skin-friction coefficient occurs after $x \approx 450\delta_{in}$, which is defined as the 'onset point'. The skin friction coefficient after transition is in good agreement with the flat-plate theory of turbulent boundary layer by Cousteix in 1989 (Ducros, 1996).

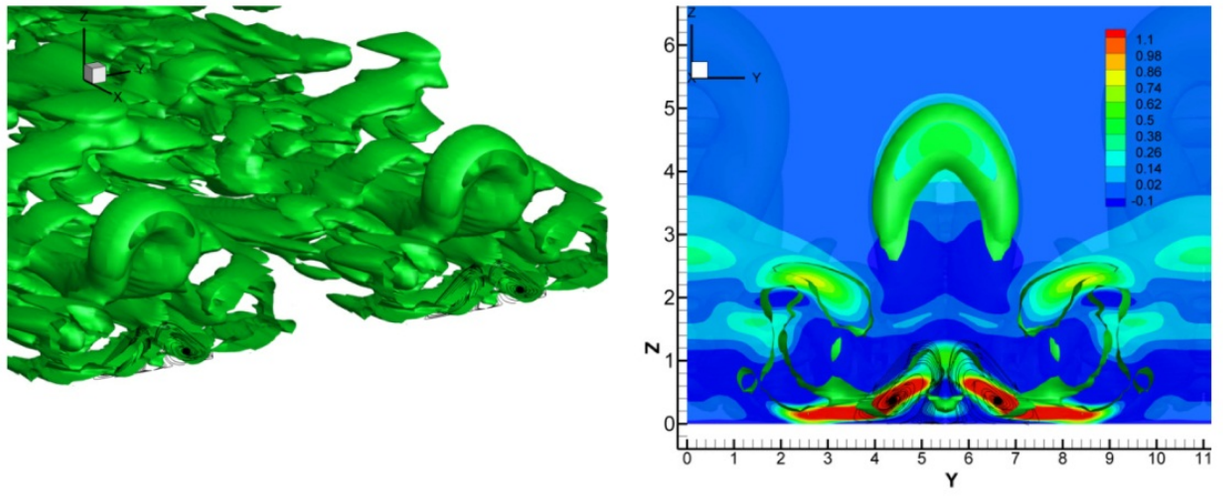

(a) (b)

Figure 10. (a)Isosurface of λ_2 (b) Isosurface of λ_2 and streamtrace at x=508.633 velocity pertubation at x=508.633

The second sweep movement [5] induced by ring-like vortices combined with first sweep generated by primary vortex legs will lead to a huge energy and momentum transformation from high energy containing inviscid zones to low energy zones near the bottom of the boundary layers. We find that although it is still laminar flow at $x \approx 450\delta_{in}$ at this time step t=8.0T, the skin-friction is immediately enlarged at the exact location where small length scales are generated, which was mentioned in last section in Fig.10. Therefore, the generation of small length scales is the only reason why the value of skin-friction is suddenly increased, which has nothing to do with the viscosity change. In order to design a device to reduce the shear stress on the surface, we should eliminate or postpone the positive spike generation, which will be discussed in more details next.

Figure12 shows the four ring-like vortices at time step t=8.0T from the side view. We concentrated on examination of relationship between the downdraft motions and small length scale vortex generation and found out the physics of the following important phenomena. When the primary vortex ring is perpendicular and perfectly circular, it will generate a strong second sweep which brings a lot of energy from the inviscid area to the bottom of the boundary layer and makes that area very active. However, when the heading primary ring is skewed and sloped but no longer perfectly circular and perpendicular, the second sweep immediately becomes weak. This phenomenon can be verified from the Figure 13 that the sweep motion is getting weak as long as the vortex rings do not keep perfectly circular and perpendicular. By looking at Figure 14 around the region of x=508, we note that there is a high speed area (red color region) under the ring-like vortex, which is caused by the strong sweep motion. However, for the ring located at x=536, we can see there is no high speed region below the first ring located at x=536 due to the weakness of the sweep motion. In addition, we can see that the structure around the ring is quite clean. This

is because the small length scale structures are rapidly damped. That gives us an idea that we can try to change the gesture and shape of the vortex rings in order to reduce the intensity of positive spikes. Eventually, the skin friction can be reduced consequently.

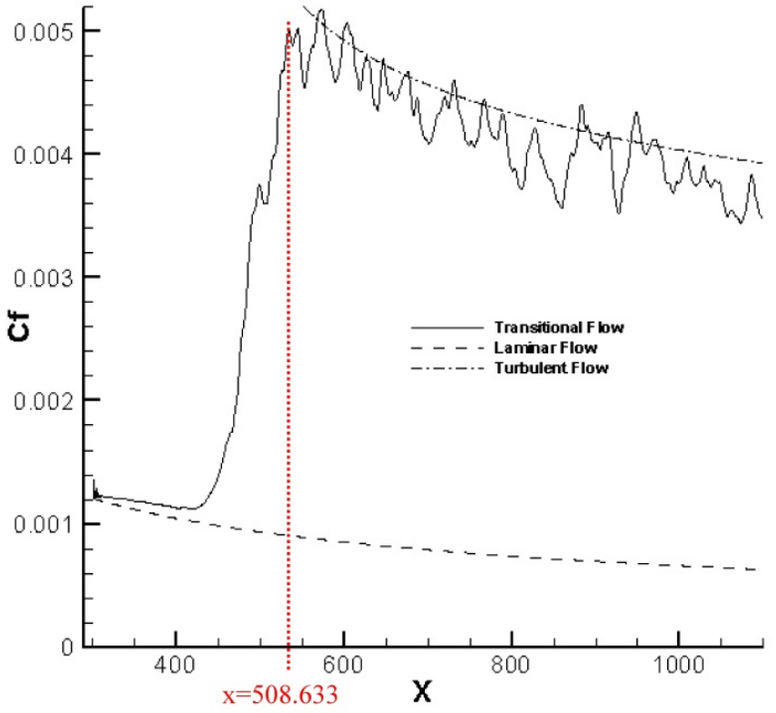

Figure 11. Streamwise evolutions of the time-and spanwise-averaged skin-friction coefficient

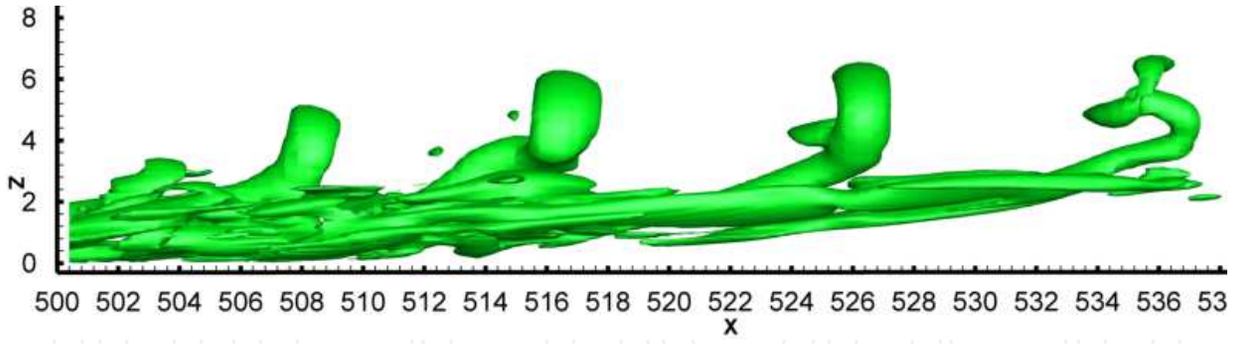

Figure 12. Side view for multiple rings at t=8.0T

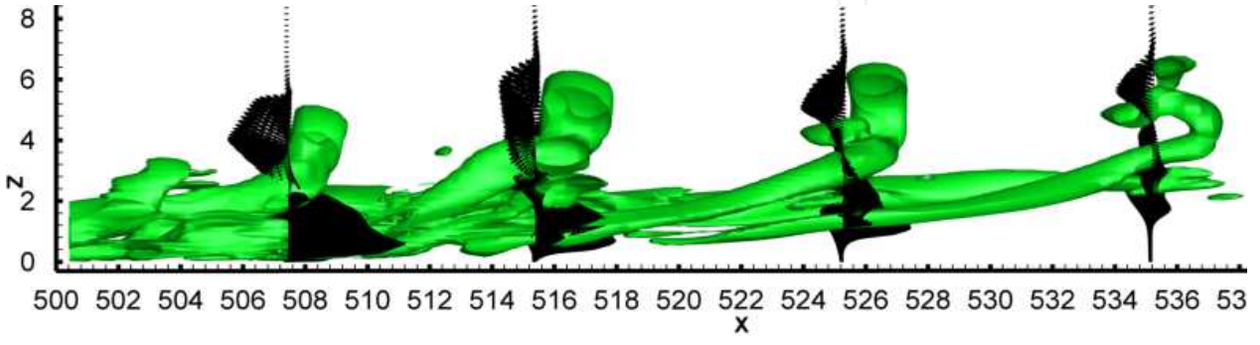

Figure 13. Side view for multiple rings with vector distribution at t=8.0T- sweep motion is weaker

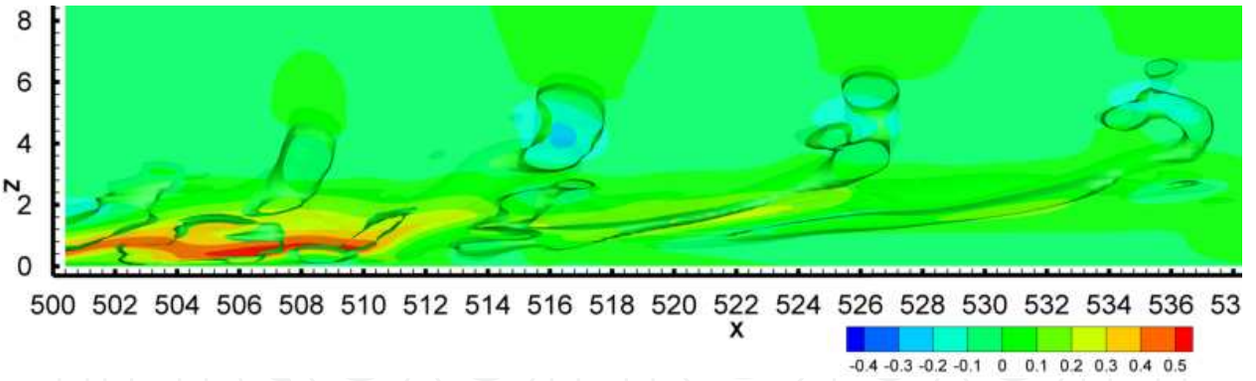

Figure 14. Side view for multiple rings with velocity perturbation at t=8.0T

6. Universal structure of turbulent flow

This section illustrates a uniform structure around each ring-like vortex existing in the flow field (Figure 15). From the λ_2 contour map and streamtrace at the section of x= 530.348 δ_{in} shown in Figure 16, we have found that the prime streamwise vorticity creates counter-rotated secondary streamwise vorticity because of the effect of the solid wall. The secondary streamwise vorticity is strengthened and the vortex detaches from the solid wall gradually. When the secondary vortex detaches from the wall, it induces new streamwise vorticity by the interaction of the secondary vortex and the solid wall, which is finally formed a tertiary streamwise vortex. The tertiary vortex is called the U-shaped vortex, which has been found by experiment and DNS. For detailed mechanisms read [10,14].

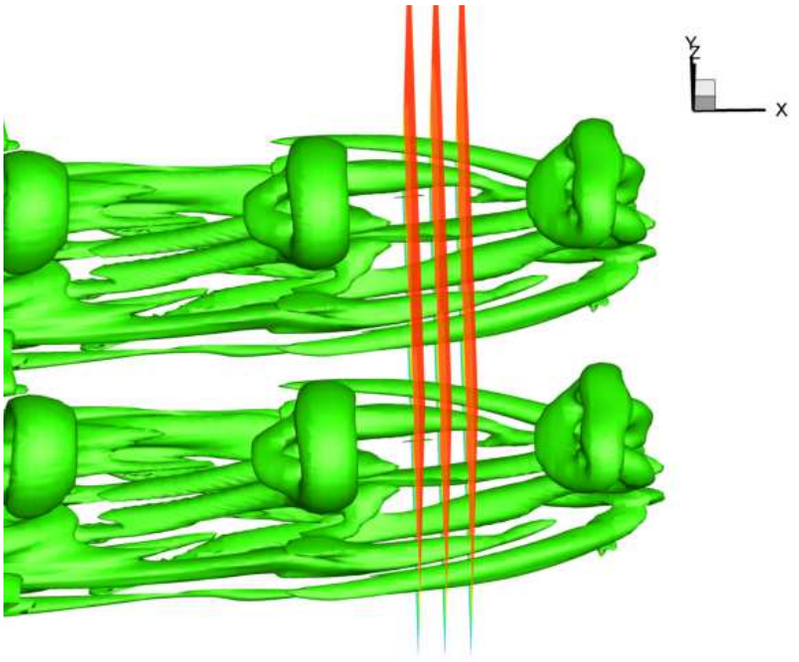

Figure 15. Top view with three cross-sections

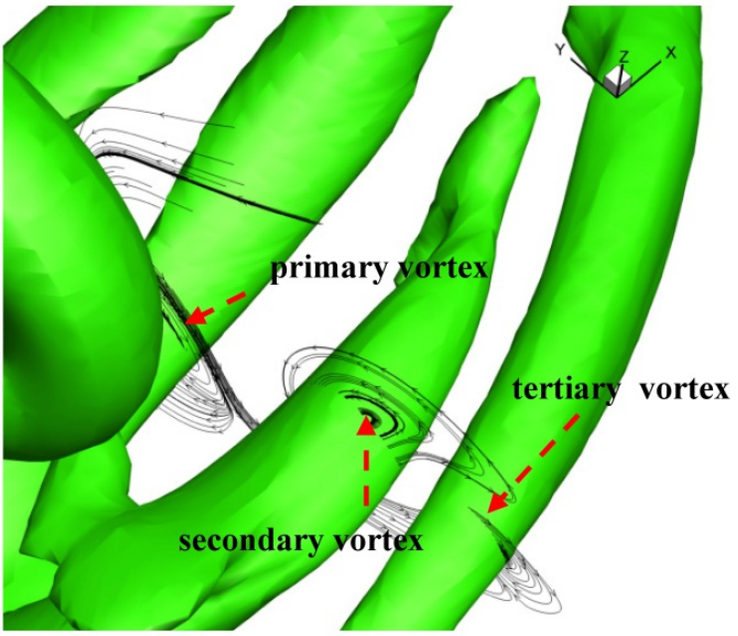

Figure 16. Structure around ring-like vortex in streamwise direction

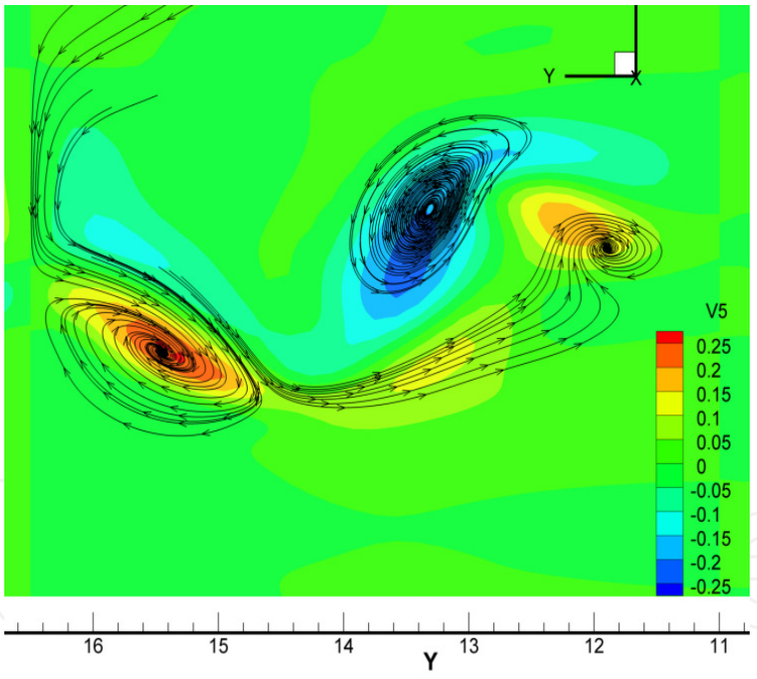

Figure 17. Stream traces velocity vector around ringlike vortex

7. Multi-level rings overlap

A side view of *isosurface of* λ_2 [8] with a cross-section at x=590 at time step t=9.2T is given in the Figure 18 which clearly illustrates that there are more than one ring-like vortex cycle overlapped together and the thickness of boundary layer becomes much thicker than before. Next, Figure 19 was obtained from the same time step and shows that there are two ring

cycles which are located at the purple frame and the red frame. This phenomenon confirms that the growth of the second cycle does not influence the first cycle which is because there is a counter-rotating vortex between those two vortex rings[14].

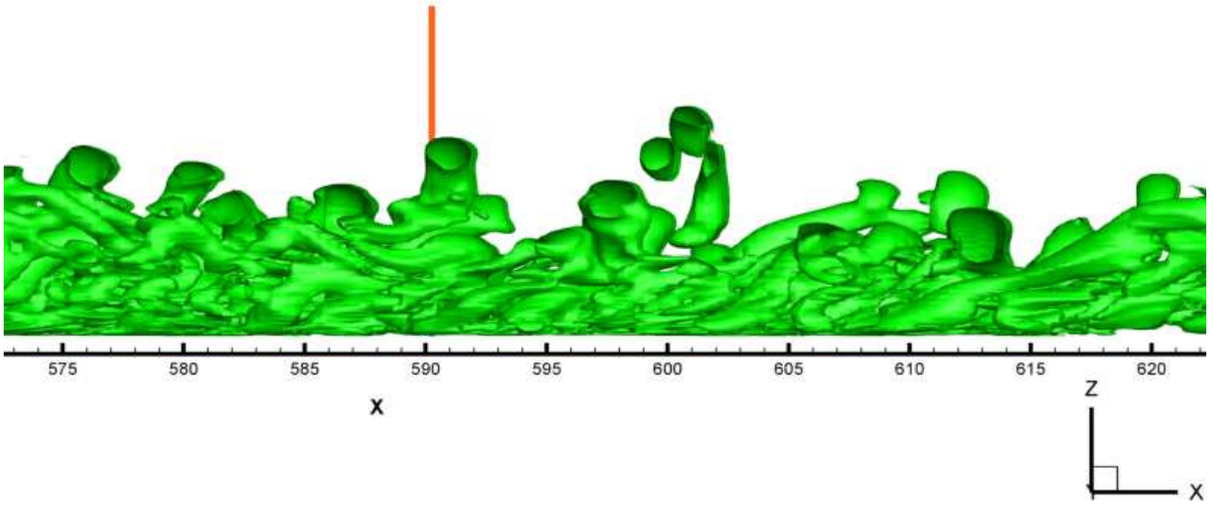

Figure 18. Side view of isosurface λ_2 with cross section

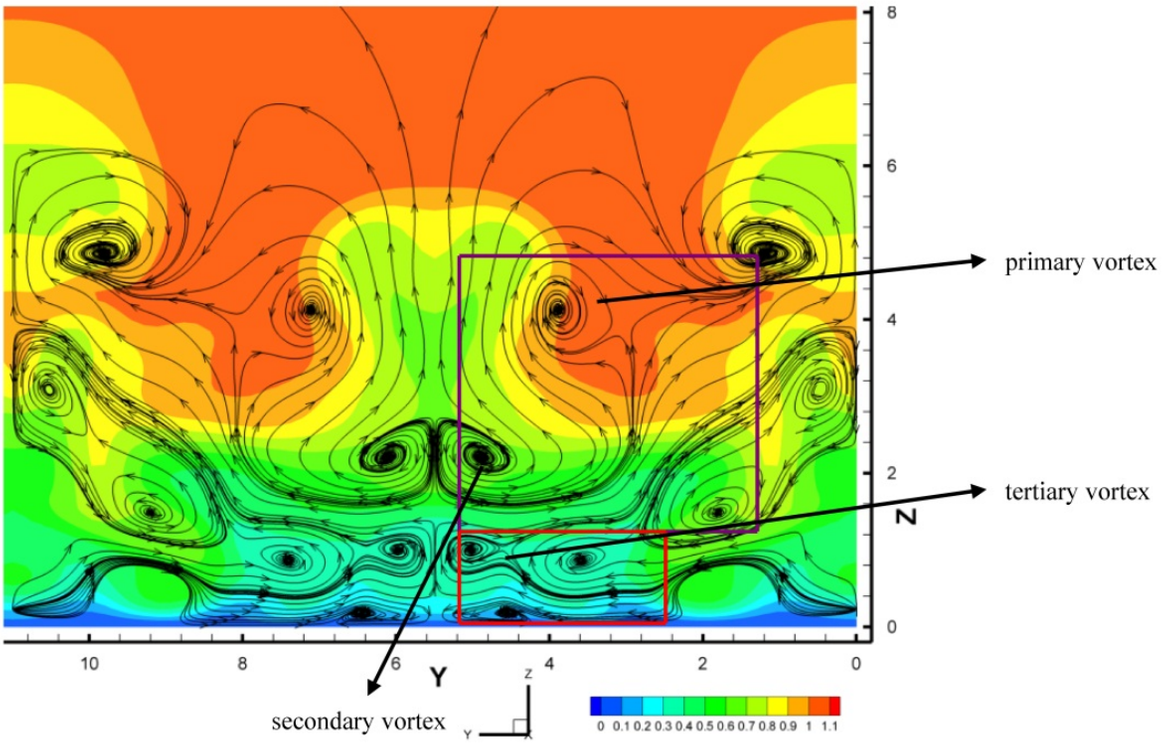

Figure 19. Cross-section of velocity distribution and streamtrace

8. Conclusion

Although flow becomes increasingly complex at the late stages of flow transition, some common patterns still can be observed which are beneficial for understanding the

mechanism that how to control the skin friction and why the boundary layer becomes thicker. Based on our new DNS study, the following conclusions can be made.

1. The skin-friction is quickly enlarged when the small length scales are generated during the transition process. It clearly illustrates that the shear stress is only related to velocity gradient rather than viscosity change.

2. If the ring is deformed and/or the standing position is inclined, the second sweep and then the positive spikes will be weakened. The consequence is that small length scales quickly damp. This is a clear clue that we should mainly consider the sharp velocity gradients for turbulence modeling instead of only considering the change of viscous coefficients in the near wall region.

3. Because the ring head moves faster than the ring legs does and more small vortices are generated near the wall region, the consequence is that the multi-level ring cycles will overlap.

4. Multiple ring cycles overlapping will lead to the thickening of the transitional boundary layer. However, they never mix each other. That is because the two different level cycles are separated by a vortex trees which has a different sign with the bottom vortex cycle.

Nomenclature

M_∞ = Mach number

Re = Reynolds number

δ_{in} = inflow displacement thickness

T_w = wall temperature

T_∞ = free stream temperature

Lz_{in} = height at inflow boundary

Lz_{out} = height at outflow boundary

Lx = length of computational domain along x direction

Ly = length of computational domain along y direction

x_{in} = distance between leading edge of flat plate and upstream boundary of computational domain

A_{2d} = amplitude of 2D inlet disturbance

A_{3d} = amplitude of 3D inlet disturbance

ω = frequency of inlet disturbance

α_{2d}, α_{3d} = two and three dimensional streamwise wave number of inlet disturbance

β = spanwise wave number of inlet disturbance

R = ideal gas constant

γ = ratio of specific heats

μ_∞ = viscosity

Author details

Ping Lu, Manoj Thapa and Chaoqun Liu
University of Texas at Arlington, Arlington, TX, USA

9. References

[1] A.Cheskidov. Theoretical skin-friction law in a turbulent boundary layer. Physics Letters A. Issues 5-6, 27 June 2005, Pages 487-494
[2] A.A.Townsend. Turbulent friction on a flat plate., Emmanuel College, Cambridge. Skinsmodelltankens meddelelse nr. 32, Mars 1954.
[3] Bake S, Meyer D, Rist U. Turbulence mechanism in Klebanoff transition:a quantitative comparison of experiment and direct numerial simulation. J.Fluid Mech, 2002 , 459:217-243
[4] Boroduln V I, Gaponenko V R, Kachanov Y S, et al. Late-stage transition boundary-Layer structure: direct numerical simulation and exerperiment. Theoret.Comput.Fluid Dynamics, 2002,15:317-337.
[5] Chen, L and Liu, C., Numerical Study on Mechanisms of Second Sweep and Positive Spikes in Transitional Flow on a Flat Plate, Journal of Computers and Fluids, Vol 40, p28-41, 2010
[6] GROSS, J. F. Skin friction and stability of a laminar binary boundary layer on a flat plate. Research memo. JAN 1963
[7] Guo, Ha; Borodulin, V.I..; Kachanov, Y.s.; Pan, C; Wang, J.J.; Lian, X.Q.; Wang, S.F., Nature of sweep and ejection events in transitional and turbulent boundary layers, J of Turbulence, August, 2010
[8] Jeong J., Hussain F. On the identification of a vortex, J. Fluid Mech. 1995, 285:69-94
[9] J.E. Sargison, et al. Experimental review of devices to artificially thicken wind tunnel boundary layers. 15th Australian Fluid Mechanics Conference.
[10] Kachanov, Y.S. On a universal mechanism of turbulence production in wall shear flows. In: Notes on Numerical Fluid Mechanics and Multidisciplinary Design. Vol. 86. Recent Results in Laminar-Turbulent Transition. — Berlin: Springer, 2003, pp. 1–12.
[11] Lee C B., Li R Q. A dominant structure in turbulent production of boundary layer transition. Journal of Turbulence, 2007, Volume 55, CHIN. PHYS. LETT. Vol. 27, No. 2 (2010) 024706, 2010b
[12] Liu, X., Chen, L., Liu, C. , Study of Mechanism of Ring-Like Vortex Formation in Late Flow Transition AIAA Paper Number 2010-1456, 2010, 2010c
[13] Liu, C. and Chen, L., Parallel DNS for Vortex Structure of Late Stages of Flow Transition, Journal of Computers and Fluids, 2010d
[14] P. Lu and C. Liu. DNS Study on Mechanism of Small Length Scale Generation in Late Boundary Layer Transition. Physica D: Nonlinear Phenomena, Volume 241, Issue 1, 1 January 2012, Pages 11-24
[15] P. Lu, Z. Wang, L. Chen and C. Liu. Numerical Study on U-shaped Vortex Formation in Late Boundary Layer Transition. Journal of Computer & Fluids, CAF-D-11-00081, 2011
[16] Schlichting, H. and Gersten, K., Boundary Layer Theory, Springer, 8th revised edition, 2000